TRIBHUVAN UNIVERSITY

INSTITUTE OF ENGINEERING

PULCHOWK CAMPUS

DESIGN AND ANALYSIS OF AN AXIAL FLOW COMPRESSOR

By:

Ankit Kharel (074BME604)

Anusha Acharya (074BME607)

Nitesh Subedi (074BME624)

Prajwal Koirala (074BME627)

A FINAL PROJECT REPORT
SUBMITTED TO THE DEPARTMENT OF MECHANICAL AND AEROSPACE ENGINEERING IN PARTIAL FULFILLMENT OF THE REQUIREMENT FOR THE DEGREE OF BACHELOR IN MECHANICAL ENGINEERING

DEPARTMENT OF MECHANICAL AND AEROSPACE ENGINEERING

LALITPUR, NEPAL

AUGUST, 2021

ABSTRACT

An axial compressor is a part of a Turbomachinery that compresses the working fluid to a higher temperature before it is combusted in the combustion chamber. The purpose of this study is to design a Turbomachinery compressor stage for the given design parameters and study the performance of the designed compressor stage using mathematical simulation. The required geometrical parameters for compressor rotor and stator are determined using fundamental theories and existing mathematical relations of Turbomachinery design principles. The design obtained is based on the NACA-65 airfoil profile which is the most widely used blade profile for axial compressor application. Finite element analysis is employed to simulate the working of the designed compressor. The designed axial compressor gives a pressure ratio of 1.1 which is somewhat less than we have expected.

ACKNOWLEDGEMENTS

We cannot express enough thanks to our professor ASST.Prof. Hari Bahadur Dura sir for providing us with the opportunity to work on this project and for his valuable insights and support throughout the whole project. We would like to thank the Department of Mechanical and Aerospace Engineering for their support and resources. We also sincerely thank our Senior Mr. Amrit Thapa without whose continuous support and motivation we would not have been able to do the work as well as we did and the whole endeavor would have been a lot more painful.

TABLE OF CONTENTS

LIST OF FIGURES

LIST OF TABLES

LIST OF SYMBOLS

φ	Flow coefficient
ψ	Work coefficient
R	Degree of reaction
α_1	Absolute flow angle at inlet
α_2	Absolute flow angle at outlet
β_1	Relative flow angle at inlet
β_2	Relative flow angle at outlet
β_{1b}	Blade angle at inlet
β_{2b}	Blade angle at outlet
δ	Deviation
θ	Camber
γ	Stagger
C	Chord
σ	Solidity
S	Spacing
N	Speed
n	Number of blades
C_a	Axial velocity
C_{anew}	New axial velocity
U_m	Peripheral velocity at mean
r	Radius
r_t	Tip radius
r_h	Hub radius

r_m	Mid radius
ρ	Density
m	Mass flow rate
U	Peripheral velocity
C_1	Absolute velocity at the inlet
C_2	Absolute velocity at the outlet
W_1	Relative velocity at the inlet
W_2	Relative velocity at the outlet
$C_{\theta 1}$	Tangential component of absolute velocity at inlet
$C_{\theta 2}$	Tangential component of absolute velocity at outlet
$W_{\theta 1}$	Tangential component of relative velocity at inlet
$W_{\theta 2}$	Tangential component of relative velocity at outlet
$\mathrm{C_p}$	Pressure Distribution coefficient
$\mathrm{M_a}$	Axial Mach number
$\mathrm{M_t}$	Tangential Mach number
$\mathrm{M_r}$	Relative Mach number
DF	Diffusion Factor
t	Thickness
i_{ref}	Reference angle of incidence

CHAPTER ONE: INTRODUCTION

1.1. Historical development

The earliest development of turbomachinery dates back more than 2000 years. The first described device is a device named Aeolipile that used steam reaction to rotate about its axis. In the subsequent years, the development of turbomachinery took place for the purposes of grinding grains and lifting. Major developments in the field of gas turbine started just before the Second Great war for the purpose of electric power development. The first major application of the gas turbine was the development of the military jet engine around the end of the war. The first jet engine-driven aircraft was de Haviland Comet introduced in 1949. These engines were initially very inefficient, noisy and unreliable but due to their huge applications jet engines saw massive development in in the 1960s and 70s where the major form of the engine was developed. In the subsequent decades, the continuous development led to the development of high bypass ratio turbofan engines, and improvement in fuel efficiency making high-capacity wide-body airlines possible. In the case of non-airlines applications, turbo engines are used as gas turbines for electricity generation. Early gas turbines for power generation applications were of low power and their thermal efficiency was too low to be competitive. By the early 21st century,

however, gas turbines were capable of outputs up to 500 MW with thermal efficiencies of over 40 per cent and the gas turbine became widely used in power generation. long-term improvements in gas turbine power and efficiency have resulted from continuous development of compressors, combined with increases in cycle temperature. The number of stages required for a given pressure ratio is important both for aircraft engines, to minimize weight, and for industrial engines, to minimize cost.

Axial-flow compressor was first patented by Sir Charles Parsons in 1884. He experimented on axial flow compressors and developed an 80-stage compressor with 70% efficiency. In his early designs, the stator guide blades were flat on one side and curved on the other, with the enlarging passage between adjoining blades serving to change the kinetic energy to air pressure. Due to poor aerodynamic design of the compressor blades, these compressors were not very efficient. The challenge of diffusing flow and stability hampered the development of axial flow compressor up until 1950s. After 1950s development in airfoil technology improved the performance of the compressors.

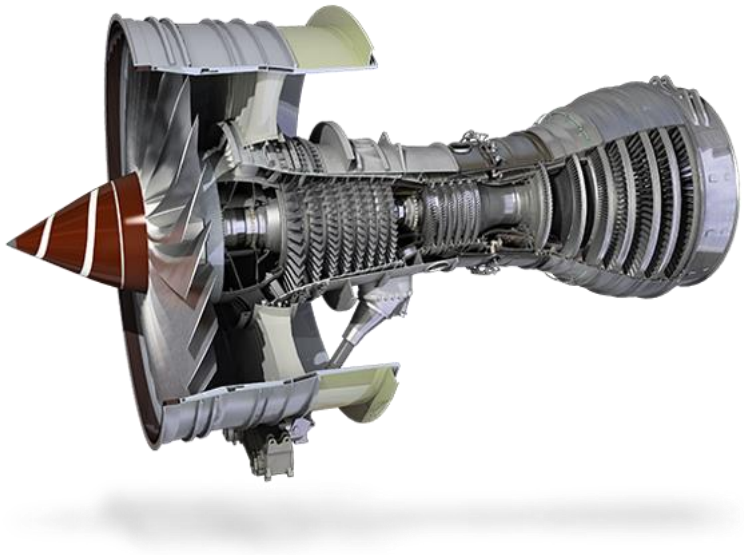

Figure 1.1: Jet Engine(RR Trent 500) (Royce, 2015)

1.2. Axial Compressor

The axial flow compressor consists of a series of stages, each stage comprising a row of rotor blades followed by a row of stator blades. The working fluid is initially accelerated by rotor blades, and then deaccelerated in the stator blade passage wherein the kinetic energy transferred to the rotor is converted to static pressure. This process is repeated in many stages as necessary for obtaining the required pressure ratio. As the compressor works in an adverse pressure gradient, the design of the compressor becomes more difficult with a high-pressure ratio. It is desirable to have a constant axial velocity throughout the compressor, that is why it is also important to have a moderate rate of change of cross-sectional area in diffusing flow as the flow progresses forward as the compression causes an increase in air density. So, blade height decreases as air progresses ahead in the compressor. Due to adverse pressure gradient, each stage of the compressor can only have a small pressure ratio as compared to the turbine working in a favorable pressure gradient. That is why compressor has a large number of stages as compared to turbines for same pressure ratio.

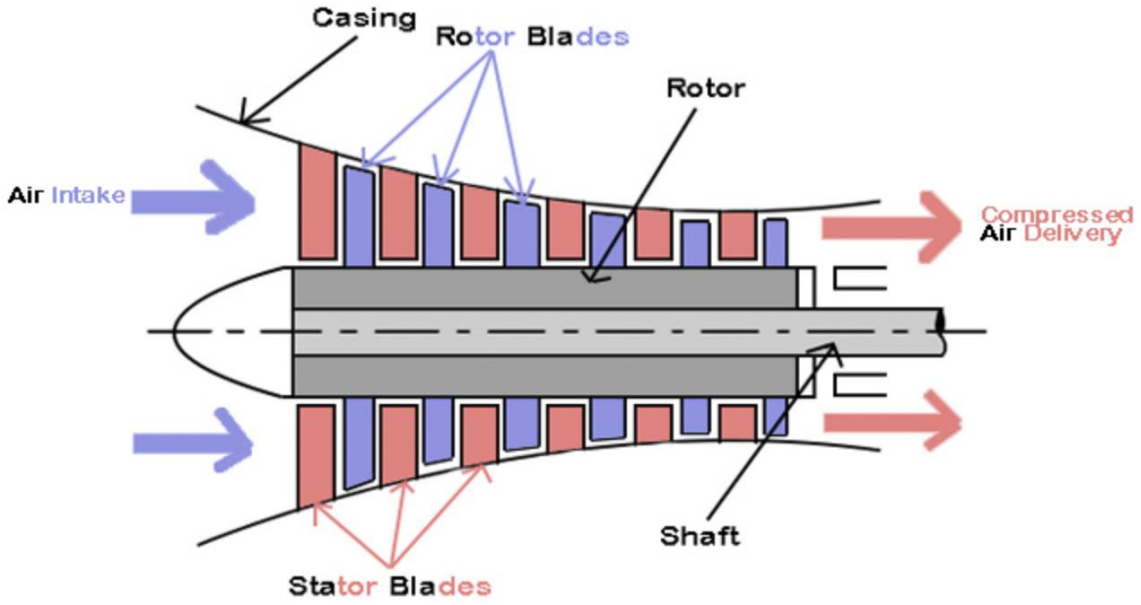

Figure 1.2: Axial Flow Compressor

The design of axial compressor is based on some overall characteristics such as mass flow rate, pressure ratio requirements, and required minimum efficiency. Also, it is generally a design aim to have minimum weight and dimension for the required application. The design of compressor blades is also based on both aerodynamic theory and experiment, to prevent the wasteful losses and also to ensure the minimum stalling troubles. The blade should turn the air through the required angle and it should carry out its diffusion process with the optimum efficiency, i.e. with a minimum loss of stagnation pressure. To minimize these losses the blade angles should be similar to the air flow angle. It should also be considered that the compressor has to operate over a wide range of speed and pressure ratio and under different operating conditions. The complete design process of axial flow compressor will encompass the following steps:

1. Choice of rotational speed and annulus dimensions
2. Determination of the number of stages, using an assumed target efficiency
3. Calculation of air angles and development of velocity triangle at the mean radius
4. Determination of velocity angle for root and tip
5. Selection of compressor blade profile
6. Checking of efficiency obtained from the designed profile
7. Testing

1.3. Objectives

1.3.1. Main objective

- To design and analyze a single stage of an axial flow compressor.

1.3.2. Specific objectives

1. To perform preliminary design.
2. To obtain the 3D model of a compressor blade.
3. To perform CFD analysis of the final design.

CHAPTER TWO: LITERATURE REVIEW

Axial flow compressor used in gas turbine applications consists of series of stages. A rotor followed by a stator comprises a single stage of an axial flow compressor. Rotor imparts kinetic energy into the fluid and this kinetic energy is converted into static pressure energy at the stator. Multistage axial flow compressor consists of 17-22 stages in advance gas turbine application (Boyce, 2012). The reason for this high number of stages is to do with the fact that, the compressor operates in an adverse pressure gradient. Pressure downstream is always higher than the upstream pressure. Therefore, fluid has to overcome this pressure gradient as it passes through an axial compressor. This limits per stage pressure ratio. Axial compressor used in industries has pressure ratio per stage ranging from 1.05 to 1.2 with a per stage efficiency of 88% to 92%. That for aerospace applications ranges from 1.15 to 1.6 with an efficiency of 80% to 85%. A higher-pressure ratio of 1.8 to 2.2 is attainable only in research applications (Boyce, 2012).

There have been great improvements in axial compressor design techniques for compressors used in aircraft gas turbine engines. In addition to increasing the efficiency, these improvements have been aimed at increasing the specific flow, the surge margin, and the pressure ratio per stage. This has allowed the development of compact, lightweight high-performance compressors and engines that are of primary importance for flight economics (Sehra et al., 1992).

A key method of increasing the cycle efficiency of a gas turbine is to increase the overall pressure ratio. Increasing the pressure ratio, or reducing the number of stages, both require a greater pressure rise per stage. This can be achieved by either increasing the blade speed or by increasing the stage loading i.e., enthalpy coefficient (Sehra et al., 1992).

2.1. Design of an axial compressor

The design process begins with the preliminary design of an axial compressor followed by a detailed 3D design of the blade. Considering essential design specifications like mass flow rate, speed, etc. base design of compressor can be created which will make up for about 60-70% of the total design process (Falck, 2008).

Ujjawal and Joshi (2013) graphically presented design steps involved in designing axial compressors in a flowchart. The authors have carried out a one-dimensional calculation of compressor also known as mean line prediction calculation, where they have determined

flow parameters along the midline height of a compressor. This design method is commonly known as the mean-line design method. For a given mass flow rate and required pressure ratio, considering axial blade velocity and speed, they have calculated the annulus dimensions. Applying free vortex condition and using the McKenzie method, stagger angle of the blade and other blade geometric parameters were calculated. In their analysis, they have considered NACA 65410 airfoil for both rotor and stator. Analytically generated Rotor and Stator blade profiles were validated using Ansys CFX. Falck (2008) and Kumar et al. (2019) also designed axial compressors following the mean line design method.

There are some general rules to follow for the design of compressor blades. Diffusion rates on the surface of the blades should be reduced as much as possible. The three-dimensional blade shape must be consistent with the operating conditions which vary along the span (Lee and Kim, 2000).

Wanjin et al. (1994) experimentally tested the leaned, positively curved, and negatively curved blade cascades. In the case of the negatively curved blade, the secondary vortical losses of the cascade were greatly reduced and the efficiency was raised.

Chen (1995) analyses the effects of turbine stator lean and skew on aerodynamics. They analyzed various shapes for stator blades, namely; Straight-leaned, Sabre-shaped, J-shaped, and S-shaped stators using a three-dimensional Navier-Stoke solver. The analysis suggested that the J-shape had the highest total mass-averaged adiabatic efficiency.

Rechter et al. (1985) tested NACA 65 and CDA profiles of blades having the same design condition under the same flow condition for stator blades and revealed the superiority of the CDA profile over the NACA 65 airfoil profile.

Boyce (2012) suggests that there have been significant changes in the design of modern axial-flow compressors. The modern design implements CDA blade profiles over NACA 65 profiles, reduced airfoil count, longer chords, high aspect ratio, smaller clearances, higher pressure ratio, high blade loading per stage, thinner leading edge, and other adjustments over previous designs.

3D Blade Design of axial compressor can be viewed either as an optimization problem or as an inverse design problem. The iterative method and the Direct method are two different types of algorithms to solve an inverse design problem. The coupled or direct method tends to find the solution of the flow field and boundary value in a single shot. Since governing

equations involved are much more complicated, we often prefer an iterative design approach where the geometry is modified in each step to obtain the desire pressure ratio. Iterative design can be carried out as a trial-and-error method. But doing so is time-consuming and computationally expensive (Madadi et al., 2015).

Madadi et al. (2015) applied the Ball-Spine algorithm (BS algorithm), a novel inverse design technique, to a three-dimensional axial flow compressor blade. In this algorithm, authors have considered duct walls as a set of virtual balls. And these balls are allowed to move freely along a specified direction which is known as the spine. To satisfy target pressure distribution, the shape of the duct is changed and the desired shape is obtained when the ball stops moving. This introduction of the physical quantity, pressure with geometry helps to increase the convergence rate of the method. The authors suggested using the BS algorithm after preliminary design, in the detailed design of the blade by satisfying parameters like lift coefficient obtained in the previous design process.

In an optimization problem, however, we determine the optimal value of design parameters. Considering weight and stall together with efficiency as the optimization objectives, Chen et al. (2005) provided an optimum design method for a subsonic axial flow compressor stage. The simulation algorithm so developed comprising of cascade geometric variables, thermodynamics compression relations, simple stress relations, and empirical loss-correlations has proven to be valid and effective.

Massardo and Satta (1990) formulated the design of an axial flow compressor stage as a nonlinear mathematical programming problem with the objective of minimizing aerodynamic losses and stage weight while increasing compressor stall margin. The problem formulation took into account both aerodynamic and mechanical limitations. The selection of design variables and constraints, as well as the computation of the objective function, were studied and reported.

Gu and Miao (1987) presented a paper, in which they had put forward an optimization flow type problem. This leads to getting the idea of the basic parameters to be considered in the optimization process. Moreover, based on optimal control theory a mathematical model of the optimal flow-type problem has been established and further recast into a typical form of optimal control problem with free initial conditions, terminal constraints, and state variable inequality constraints. The physical model gives a detailed idea of the

compressor rotor blade design variables along with boundary constraints and finally the mathematical expression of the optimal flow problem.

Komarov et al. (2014) used structured topology of the airfoil together with modern CFD and optimization algorithms to find the best blade profile for the given specifications. This led to improvement in 8 degrees of turning angle with the same level of losses as for the initial design. Also, a possible design is provided for a 12-degree gain in turning angle with higher pressure losses of 20% (relatively).

Lee and Kim (2000) proposed a new technique for the optimization of the compressor blades. They put forward the idea to couple numerical optimization techniques with 3-dimensional thin layer Navier stokes solver. The design thus observed was verified with the first stage of the four-stage ATKOM compressor designed by Noel Penny Turbines (NPT) and the result showed that the efficiency was increased by 1.1 percent. The total pressure rise across both rotor and stator was increased. The flow field at the stator exit showed that the effect of wakes was also suppressed

Bloch and O'Brien (1992) created a model for predicting the wide flow range characteristics of axial flow compressor stages and studied the influence of altering design factors on steady-state performance using a parametric analysis. The model was successfully applied to a 3-stage low-speed compressor and a 10-stage high-speed compressor with mixed results. He came to findings on how stalling started and the impact of running a stage in a multistage system.

2.2. CFD analysis of an axial compressor

Bringhenti et al. (2015) presented a procedure for the CFD analysis of turbines and provided guidelines for CFD analysis of general turbomachinery. Description of turbulence and selection of turbulence model is a key problem while conducting CFD or numerical analysis of complex flow. We will require a refined turbulence model to accurately predict different cases like separating flows, flows strongly affected by secondary flows, rotating flows, etc. Mamidoju (2014) analyzed a multistage axial compressor using Ansys CFX and made a comparison between the k-epsilon and SST models. In this paper effective grid was generated by varying y-plus value and the number of nodes in the O-grid region. For the meshing of the curved surface in turbomachinery

author suggested a “multi-block hexahedral structured grid”. For upstream and downstream of the blade, a combination of H/J type of topology was used, and around the blade profile, O-grid topology was used to obtained excellent boundary layer resolution.

Simoes et al. (2009) used $k-\epsilon$, $k-\omega$, and SST turbulence models to determine the flow field of an axial flow compressor, and compared the results obtained with the experimental data. SST model was found to be more closer to the experimental data. Therefore, the authors concluded that the SST model is the most appropriate model for the simulation of an axial flow compressor.

CHAPTER THREE: METHODOLOGY

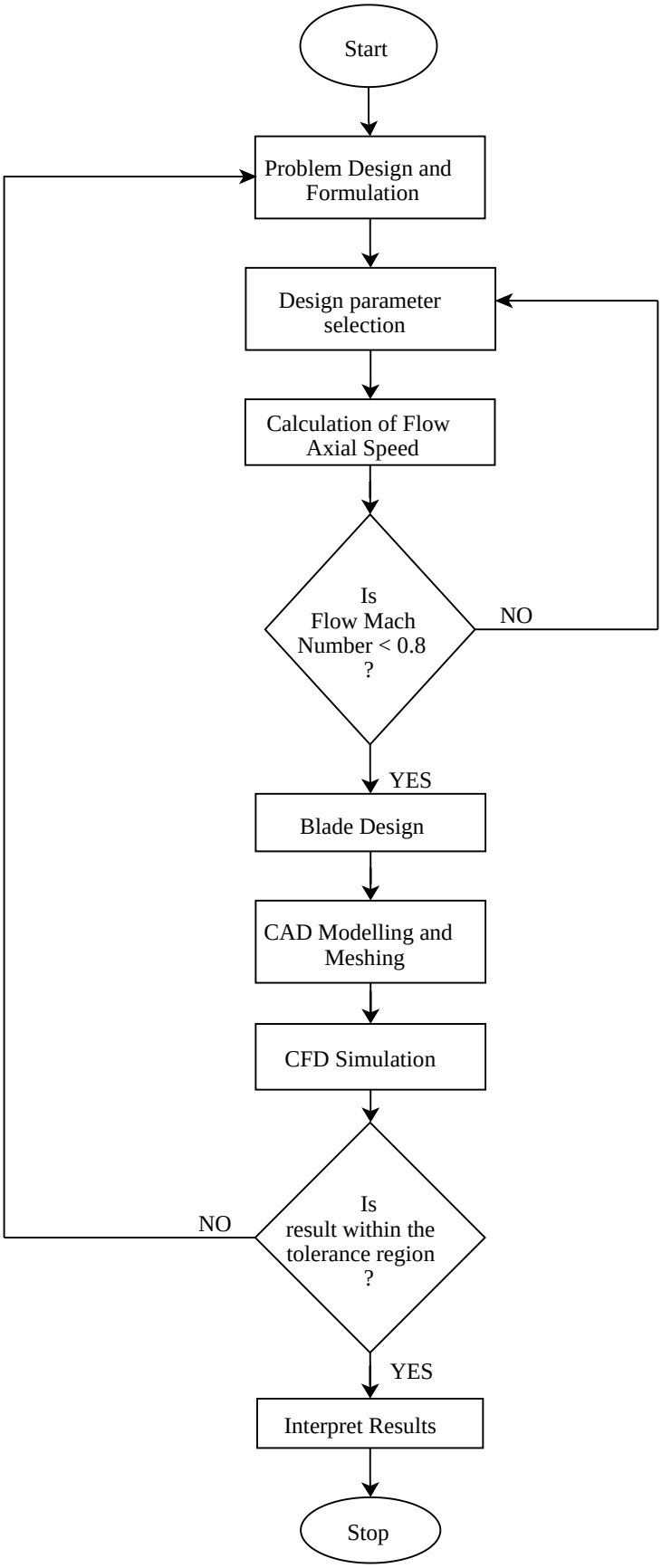

Figure 3.1 Methodology flow chart

3.1. Problem Design

We design an axial compressor for the values of parameters given in Table 3.1. It should be noted that rotor speed is corrected later in our design process to make flow at the compressor completely subsonic. However, for the initial iteration following the literature, the value shown in Table 3.1 was taken.

Table 3.1 Design specification

Parameters	**Values**
Mass flow rate	4.91 kg/s
Rotor speed	27000 rpm
Inlet temperature	288 K
Inlet pressure	1 bar

3.2. Preliminary Design

Design of axial-flow compressor is done in two stages: Preliminary and detailed design steps. Preliminary design procedure performs inverse task calculations i.e., flow geometry is calculated based on the boundary condition (Salunke et al., 2014). First, the preliminary aerodynamic design is conducted. In this step, features of the compressors such as a number of stages, speed, blade loading, annulus size, geometric blade profiles are determined and the initial geometry of the blade is constructed. This is done on the basis of a set of previously identified design variables. The constraints imposed on the design are examined and checked for if they are satisfied. If any of the constraints are not satisfied, the design variables are re-analyzed and modified to meet the constraints. In this step, aerodynamic and geometrical features of axial compressors are generated. Later the preliminary design is tested for performance analysis and some or all of the design variables are modified if the design does not satisfy the predetermined design performances.

3.2.1. Design parameters selection

The first step in the preliminary design of the axial flow compressor is to set the values of the following four input parameters at mean diameter.

- The flow coefficient, φ

- The work coefficient, ψ
- The degree of reaction, R
- The stage efficiency (isentropic or polytropic efficiency)

Gambini and Vellini (2020) suggested the use of a smith diagram to determine the work and flow coefficient. The effective range of work coefficient is 0.2-0.45 and that for flow coefficient is 0.4-0.8. Taking the work coefficient as 0.4, the degree of reaction can be calculated from Equation 2.

$$tan\alpha_1 = \frac{1 - R - \frac{\psi}{2}}{\varphi} \qquad \text{Equation 1}$$

For $\alpha_1 = \alpha_3 = 0, R\ reduces\ to$:

$$R_{\alpha_1=0} = 1 - \frac{\psi}{2} \qquad \text{Equation 2}$$

Flow coefficient can be obtained from the following empirical relation developed by Aungier (Gambini and Vellini, 2020).

$$\varphi = \frac{\pi}{4} \cdot \left[\frac{\frac{\psi}{k} - R^* \cdot \frac{6}{17}}{0.86} \cdot \left(\frac{R^*}{0.5} \right)^{1.18} \right]^{\frac{1}{2 + \frac{1}{R^*}}} \qquad \text{Equation 3}$$

Where, $R^* = 0.5 + |R - 0.5|$

k = 0.8 (20% stall margin)

From the smith diagram, initial stage efficiency is obtained as 91%.

3.2.2. Calculation of flow angles at mean line

Once we have the value of three independent parameters $\varphi, \psi\ and\ R$, all flow angles can be determined with the help of kinematic empirical Equations (4-6).

$$tan\alpha_2 = \frac{1 - R + \frac{\psi}{2}}{\varphi} \qquad \text{Equation 4}$$

$$tan\beta_1 = \frac{R + \frac{\psi}{2}}{\varphi}$$ Equation 5

$$tan\beta_2 = \frac{R - \frac{\psi}{2}}{\varphi}$$ Equation 6

3.2.3. Selection of compressor speed

In actual practice for any gas turbine application, the speed of the compressor is the same as that of the turbine. Whereas, in our design, we aim to make sure the flow through the compressor is in the subsonic region. Hence, we analyzed the rotor speed at various initial speeds using mean line analysis. For the initial speed of 27,000 rpm, the tangential Mach number at mean is found to be 0.997 meaning the flow in the compressor is transonic. For a speed of 10,000 rpm, the relative Mach number at mean is found to be about 0.68 and that for tip is around 0.75 which is determined to be appropriate for our design objective. Therefore, a rotor speed of 10,000 rpm is considered. Following steps were adopted for the selection of compressor speed.

1. Consider the initial value of speed N from literature.
2. Calculate axial velocity, refer to MATLAB "axial_velocity" function.
3. Formulate velocity triangle, refer to MATLAB "veltr" function.
4. If relative Mach number at tip < 0.8 then N is taken
5. Else consider the new speed and repeat the process until it satisfies step 4.

3.2.4. Calculation of axial velocity

Blade tip to hub ratio is selected to be 0.5. Now, using isentropic relations and cycle efficiency we can determine the basic annulus dimensions of the compressor. The axial velocity in most cases is assumed to have a certain value. In our case, we have run an iterative function "axial_velocity" in MATLAB to get axial velocity. The function algorithm is as follows:

1. Assume initial axial velocity, C_a
2. Calculate hub, tip and mean radius, and mean rotor velocity, r_t, r_h, r_m, U_m
3. Calculate $C_{anew} = U_m * \varphi$
4. If $|C_a - C_{anew}| \leq err\ then\ C_{anew}\ is\ taken$
5. Else go to step 2 and repeat the process until convergence.

The necessary geometric condition was determined using Equations (7–10). Tip clearance can be calculated with the help of Equations (11-12)

$$r_t^2 = \frac{m}{\pi . \rho . C_a \left[1 - \left(\frac{r_h}{r_t}\right)^2\right]} \quad \text{Equation 7}$$

$$\mathrm{r_h} = \mathrm{r_t} * \frac{\mathrm{r_h}}{\mathrm{r_t}} \quad \text{Equation 8}$$

$$r_m = \frac{r_t + r_h}{2} \quad \text{Equation 9}$$

$$U_m = \frac{2 * \pi * r_m * RPM}{60} \quad \text{Equation 10}$$

$$span = r_t - r_h \quad \text{Equation 11}$$

$$Tip\ clearance\ (t_c) = 5\%\ of\ span \quad \text{Equation 12}$$

3.2.5. Mean line analysis

The rotor velocity components are obtained as follows:

$$C_1 = \frac{C_a}{\cos(\alpha_1)} = C_a \quad \text{Equation 13}$$

$$W_{\theta 1} = C_a \times \tan(\beta_1) \quad \text{Equation 14}$$

$$C_{\theta 2} = C_a \times \tan(\alpha_2) \quad \text{Equation 15}$$

$$W_{\theta 2} = C_a \times \tan(\beta_2) \quad \text{Equation 16}$$

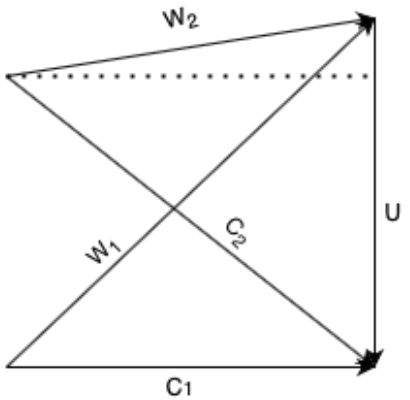

Figure 3.2: Velocity diagram at mean

The values of three design parameters $\varphi, \psi \; and \; R$ were again recalculated using the following Equations. Here, the value obtained from the velocity triangle was used.

$$R = \frac{1}{2} - \left(\frac{C_a}{U}\right)\frac{(\tan(\beta_2) + \tan(\alpha_1))}{2} \quad \text{Equation 17}$$

$$\varphi = \frac{C_a}{U} \quad \text{Equation 18}$$

$$\psi = \frac{C_{\theta 2} - C_{\theta 1}}{2} = 1 + \left(\frac{C_a}{U}\right)(\tan(\beta_2) - \tan(\alpha_1)) \quad \text{Equation 19}$$

Calculated values fall within the tolerance error. Therefore, we proceed forward in the design step. Applying the Euler turbomachinery equation, the minimum power required can now be obtained.

$$\text{Minimum power required} = \mathrm{U}(\mathrm{C}_{\theta 2} - \mathrm{C}_{\theta 1}) \quad \text{Equation 20}$$

As the ratio of relative velocities was greater than 0.658, the McKenzie method was used to calculate solidity.

$$\frac{\mathrm{S}}{\mathrm{C}} = \frac{1}{\sigma} = 9\left(0.567 - \mathrm{C_p}\right) \quad \text{Equation 21}$$

Where,

$$\mathrm{C_p} = 1 - \left(\frac{\mathrm{W_2}}{\mathrm{W_1}}\right)^2 \quad \text{Equation 22}$$

Since the blade height and solidity are known, these parameters help to determine the geometry of the channel gap and hence the number of blades required.

$$\text{Number of blades (n)} = \frac{2\pi r_m}{S} \quad \text{Equation 23}$$

Applying free vortex law ($C_\theta . r = constant$) at both inlet and outlet of the hub and the tip sections, velocity components at the hub and the tip of the blades along with their angular orientation can be calculated. It is of utmost importance to calculate the Mach number at the tip as the flow might be supersonic while dealing with a high-speed compressor.

$$\text{Axial Mach number } (\mathrm{M_a}) = \frac{\mathrm{C_a}}{\mathrm{a}} \quad \text{Equation 24}$$

$$\text{Tangential Mach Number } (M_t) = \frac{U}{a} \quad \text{Equation 25}$$

$$\text{Relative Mach number } (M_r) = \sqrt{M_a^2 + M_t^2} \quad \text{Equation 26}$$

Using Equations (23–25), M_r at the tip is found to be 0.745, therefore NACA 65 series airfoils were considered for blade profile. From cascade data, refer to Appendix, NACA 65-1210 was found to be best suited for our application. However, in the design process, we have considered NACA 65-410 airfoil and constant chord from hub to tip.

3.3. Blade angle calculation

The change in peripheral velocity from hub to tip demands the blade to be staggered at a proper angle for maximum extraction of energy. However, determining blade angles and stagger angle is an iterative process. A MATLAB code, function named "blade_angle" was used to calculate required blading dimensions such as camber, deviation angle, stagger angle, etc. Blade angles were calculated by using empirical relations given by Falck (2008) following the algorithm:

1. Assume initial camber, θ
2. Calculate $i_{ref}, \delta_{i=i_{ref}}, \beta_{b1}, \beta_{b2}$ using empirical relations.
3. Calculate $\theta_{new} = \beta_{b1} - \beta_{b2}$
4. If $|\theta - \theta_{new}| \leq err$ *then* θ_{new} *is taken*
5. Else go to step 2 and repeat the process until convergence.

To calculate the stagger angle(γ) of the blade following expression (Aungier 2003) is used:

$$\gamma = \beta_1 - \left[3.6 \times K_t + 0.3532 \times \theta \times \left(\frac{l}{c}\right)^{0.25}\right] \times (\sigma)^{0.65-0.02\times\theta} \quad \text{Equation 27}$$

Where:

$$K_t = \left(10 \times \frac{t_{max}}{C}\right)^{\frac{0.28}{0.1+(t_{max}/C)^{0.3}}} \quad \text{Equation 28}$$

Where:

$$\frac{l}{c} = 0.5, \text{ and } \frac{t_{max}}{c} = 0.1$$

The stator blade is designed similarly to the rotor blade. The same blade profile as the rotor is selected for the stator as well. The aspect ratio of the stator blade is selected to be 2.5. Knowing the values of aspect ratio and for the same blade height of the stator blade as the rotor blade, the blade chord is calculated. The axial distance between stator and rotor is taken as 20% of rotor chord length.

$$Axial\ gap = 0.2 \times C \qquad \text{Equation 29}$$

3.4. CAD design

After obtaining geometric parameters from preliminary analysis and blade setting angle, a single-stage axial compressor was modeled using SolidWorks. The calculation for three locations of the rotor and stator, at hub, mid, and tip, both were performed and required design variables were then used for the modeling. A simple loft feature was used for making 3d rotor out of the profiles calculated.

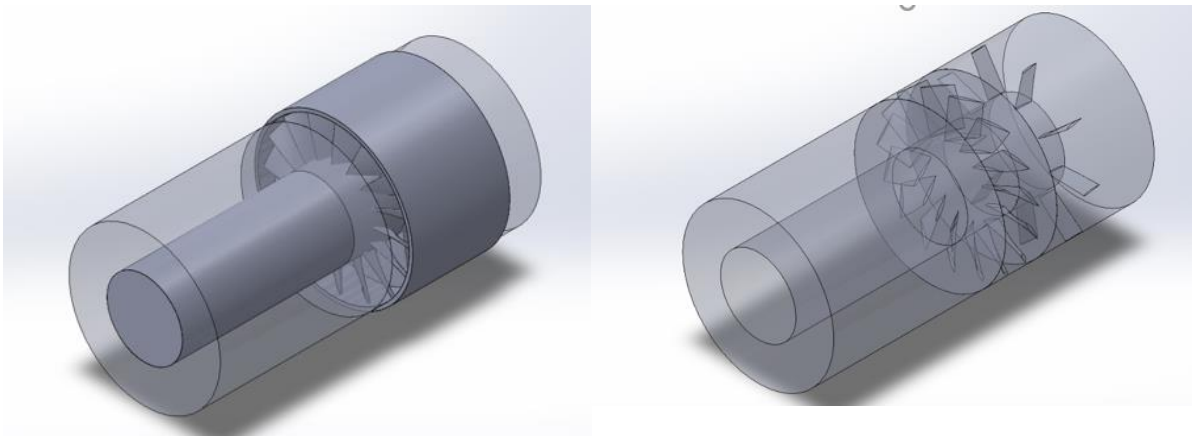

Figure 3.3 CAD modeling

3.5. Meshing

For the meshing in fluent, 3 domains are created- 1 rotating domain and the other non-rotating. The rotating domain is for the rotor section and the other domain is for the inlet and stator section as shown in the figure below.

For the meshing of the compressor, fluent meshing was preferred. The mesh was created for the inlet domain but for the rotor and stator domain, we were unable to make a mesh with an element size of 3mm. The mesh quality was very low in those sections and one of the possible remedies is to decrease the mesh size to capture the curvature of the airfoil profile but below 3mm we were unable to mesh as our pcs hung up during the process. We

are now looking for a more powerful PC or if possible, make a manual mesh in ICEM CFD. Currently, we also tried automatic meshing with ICEM, but the result was very poor.

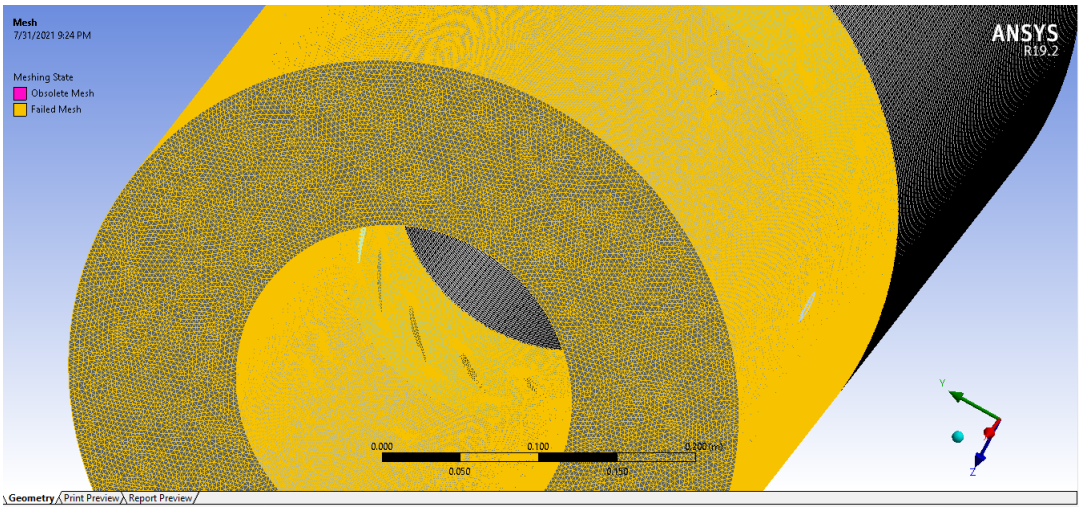

Figure 3.4 Meshing

3.4. Simulation and Analysis

Once a detailed CAD model is prepared, it is subjected to computational fluid dynamic simulation and analysis. If the simulation results are not satisfactory enough, the design optimization process is reiterated by re-performing a detailed design. Since the final design is highly dependent on the results of the aerodynamic preliminary design, it is a critical phase in the axial compressor design. Thus, it might be required to restart from the preliminary design if deemed necessary by the simulation results.

CHAPTER FOUR: RESULTS AND DISCUSSION

Following the design methodology, the values obtained for the various parameters are presented in this chapter.

Table 4.1 Values of the Input Parameters

Parameters	**Values**
Degree of reaction (R)	0.8
Work coefficient (ψ)	0.4
flow coefficient (φ)	0.61

Table 4.1 shows the values of three input parameters. Degree of reaction near 0.5 is considered to be optimal, but to satisfy Equation 2 doing so would provide an unacceptable value of work coefficient which is 1. This indicates that to obtain the value of R near 0.5, we require an Inlet guide vane that directs the incoming at a certain angle.

The corrected design parameters and geometric parameters obtained from the preliminary design are presented in Table 4.2. Table 4.3 shows the values of different components of the velocity triangle. It is clearly seen that the absolute velocity of flow increases when it passes through the rotor. But, the relative flow at the outlet decreases. This decrease in the relative component of velocity compensates for a rise in pressure at the rotor. Therefore, some diffusion is also obtained in the rotor and the value of DF is found to be 0.42. The velocity triangle diagram can be obtained by substituting the values presented in Table 4.3 in Figure 3.2.

Table 4.4 presents various blade and flow angles associated with the rotor. The solidity of a rotor blade is varied from 1.69 at the hub, 1.1 at mid to 0.844 at the tip. This implies that since the gap between two consecutive blades at the hub is less than of tip, flow at the hub is more influenced or affected by the other successive blades. Solidity for stator is found to be 0.57,0.35, and 0.28 at hub, mid, and tip respectively.

Table 4.5 presents the variation of Mach number from hub to tip. The Mach number is greater than 0.3 so the flow in our compressor is compressible. Mach number increases

from hub to tip because of an increase in tangential Mach number which is a function of peripheral velocity.

Table 4.2 Rotor and Stator design and geometric parameters

Parameters	**Values**
Corrected rotor speed (N)	10000 RPM
Blade to tip ratio	0.5
Aspect ratio of rotor	1.5
Aspect ratio of stator	2.5
Axial velocity (C_a)	105.416 m/s
Tip Radius (r_t)	0.22m
Hub Radius (r_h)	0.11m
Mean Radius (r_m)	0.165m
Span	0.11m
Tip clearance (5% of span)	0.006m
Radius inlet	0.226m
Number of rotor blades	16
Number of stator blades	9 (8 used in simulation)
Axial gap	0.015m
Chord of stator	0.045 m
Chord of rotor	0.0733m
Minimum power required	10573.1 Watts

Table 4.3 Values of different components of velocity triangle

Parameters	**Values**		
	Hub	**Mid**	**Tip**
U	115.21 m/s	172.814 m/s	230.42 m/s
C_1	105.416 m/s	105.416 m/s	105.416 m/s

W_1	$156.159 m/s$	$202.389\ m/s$	$253.387 m/s$
$C2$	$139.766\ m/s$	$121.884\ m/s$	$114.97\ m/s$
W_2	$107.99\ \ m/s$	$147.848\ \ m/s$	$212.52\ \ m/s$

Table 4.4: Parameters of the rotor at hub, mid, and tip

Parameters	**Hub**	**Mid**	**Tip**
α_1	0	0	0
α_2	41.04°	30.13°	23.52°
β_1	47.54°	58.61°	65.42°
β_2	12.53°	44.52°	60.26°
β_{1b}	48.558°	60.069	64.301
β_{2b}	5.78	37.510	56.027
δ	7.33°	7.010°	4.233°
θ	42.772°	22.551°	8.267°
γ	31.123°	45.762°	57.703°
c	0.0733 m	0.0733 m	0.0733 m
σ	1.6976	1.1039	0.8488

Table 4.5 Mach number variation from hub to tip

Mach Number	**Hub**	**Mid**	**Tip**
Axial Mach Number	0.3099	0.3099	0.3099
Tangential Mach Number	0.3387	0.508	0.6774
Relative Mach Number	0.459	0.5961	0.745

Table 4.6 Mesh Characteristics

Number of Nodes	888559
Number of Elements	4885714

Table 4.7 Solution setup

Analysis Type	Steady-state
Fluid	Air Ideal Gas
Energy Equation	On
Turbulence	Shear Stress Transport
Resuidal	10^{-4}

Table 4.8 Boundary condition at different sections of the fluid domain

Boundary Condition	**Type**
inlet	Mass-Flow-Inlet
inlet_wall_inner	Wall
inlet_wall_outer	Wall (No slip)
outlet	Outflow
rotor	Wall
rotor_wall_inner	Wall
rotor_wall_outer	Wall (No slip)
stator	Wall (No slip)
stator_wall_inner	Wall
stator_wall_outer	Wall (No slip)

Here, all the outer walls are stationary and all the inner walls are moving walls with rotation components along the -x axis with a speed of 1049 rad/s. Also, the rotor is specified as a moving wall and the stator is stationary.

Applying mass flow rate at inlet solution obtained from simulation is presented in Figure (4.1 to 4.5). Variation of velocity from hub to tip can be visualized with the help of Figure. Absolute velocity increases from hub to tip as it is a function of radius. Here we can also observe that the value obtained from the simulation also matches the result obtained from the preliminary calculation. By observing the pressure contour at rotor blades, we can see that static pressure remains almost constant along the radial direction. This verifies the free vortex law assumption.

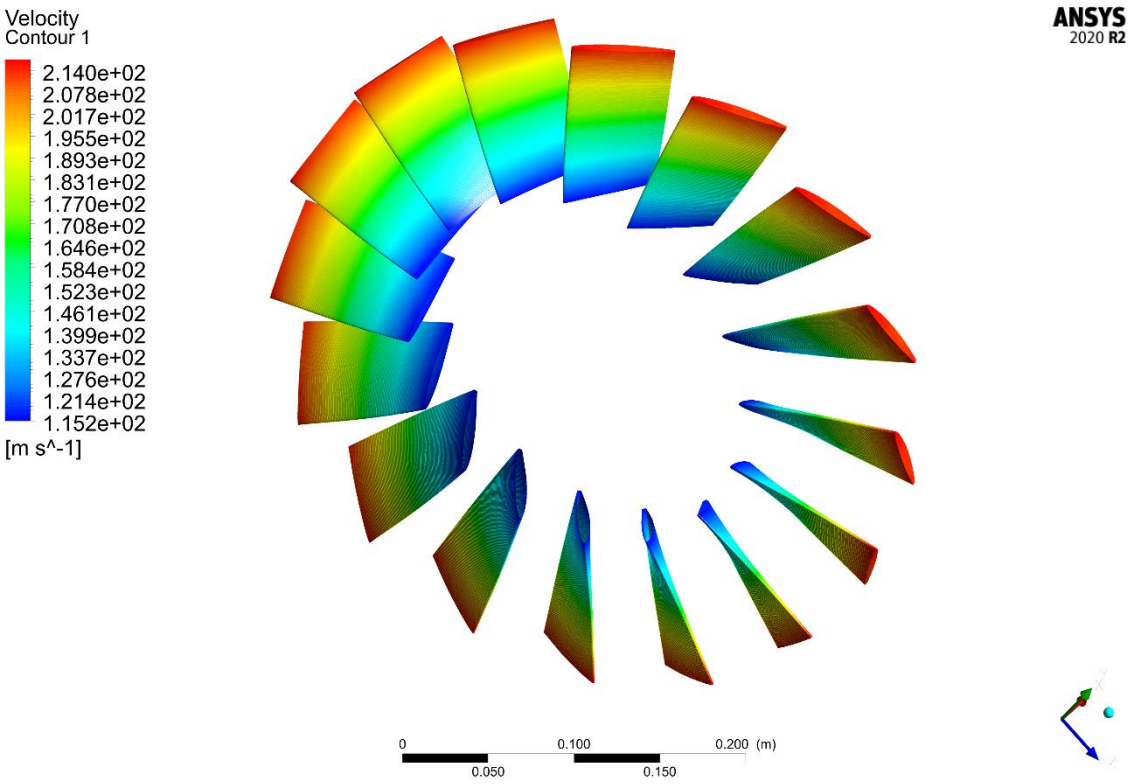

Figure 4.1 Velocity Contour of Rotor baldes

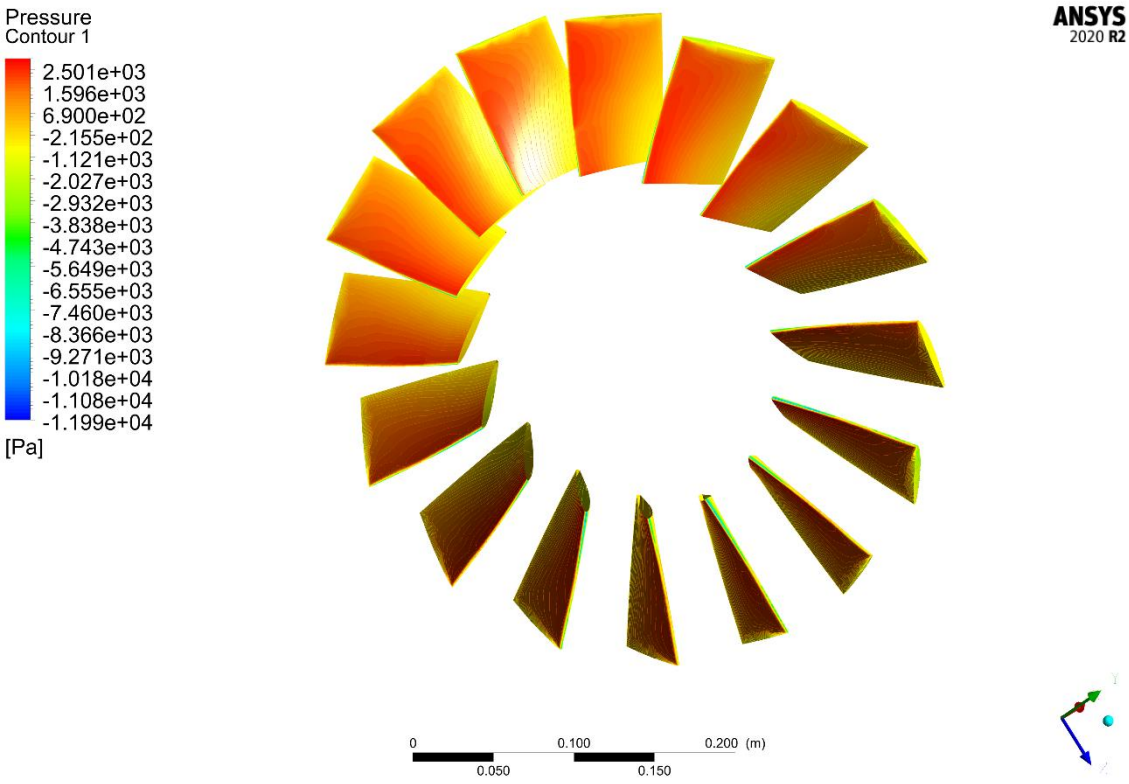

Figure 4.2 Pressure contour of Rotor blades

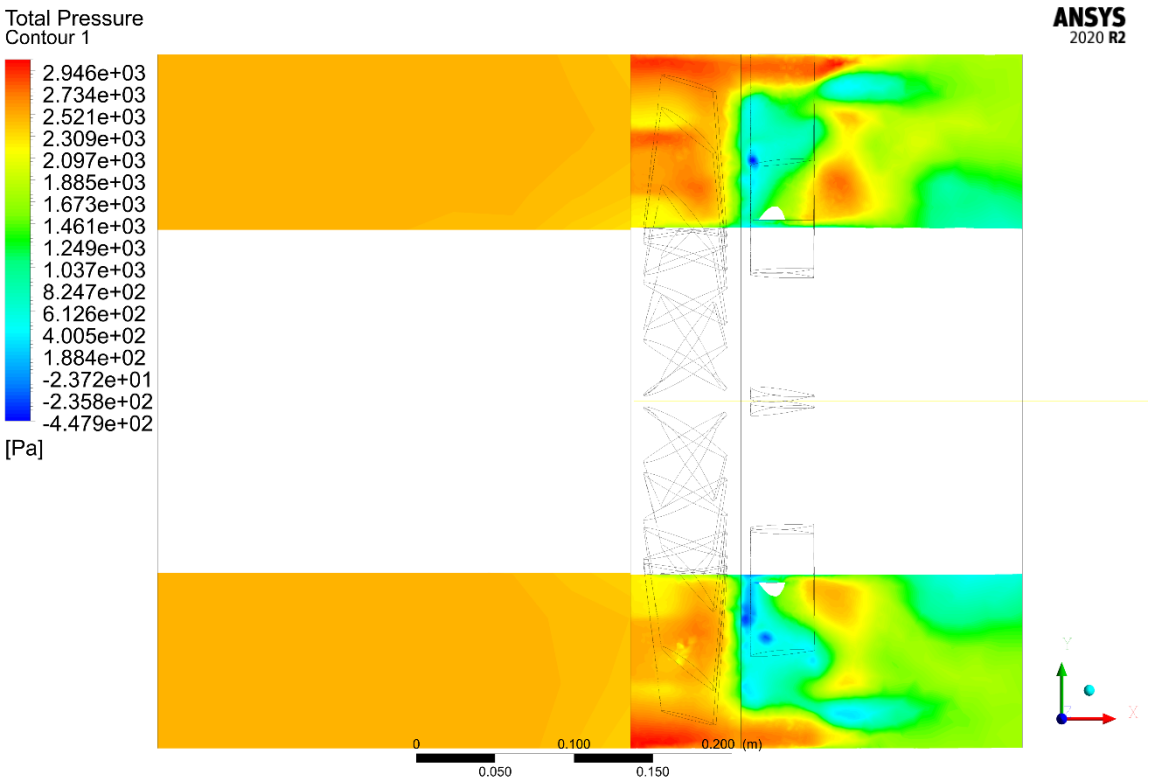

Figure 4.3 Variation of total pressure throughout the flow domain

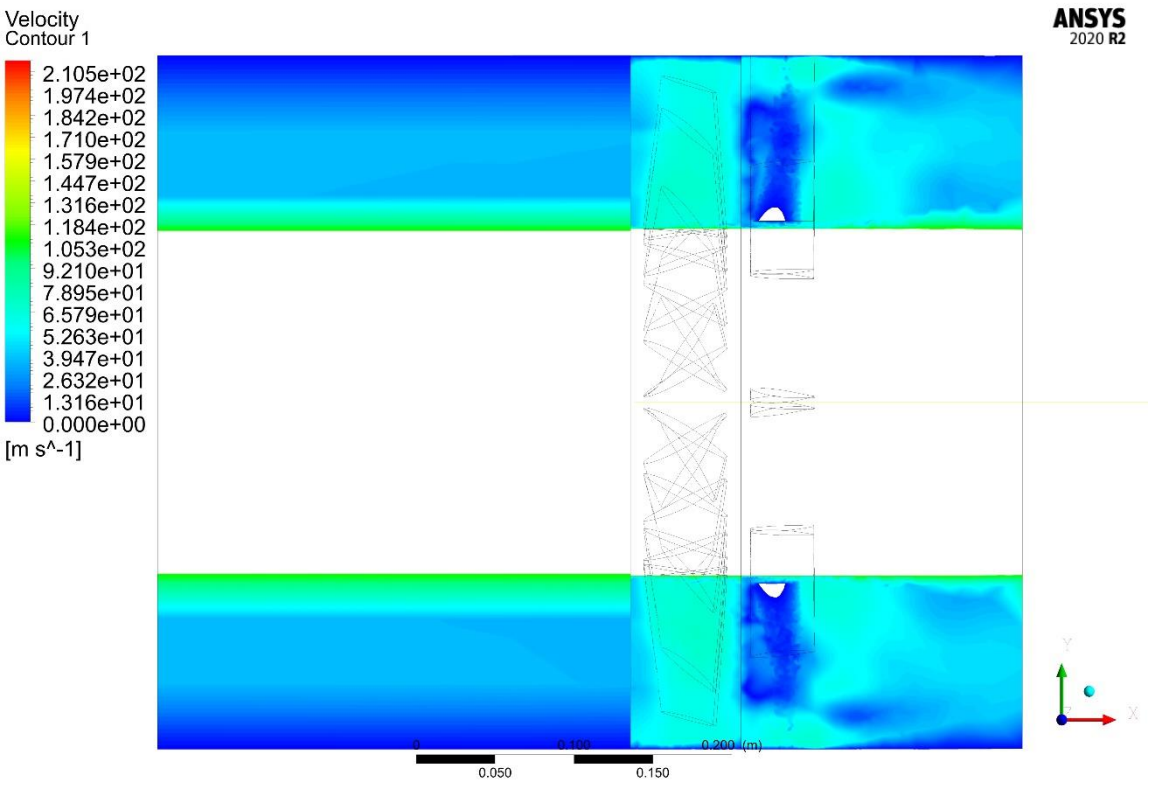

Figure 4.4 Variation of absolute velocity throughout the flow domain

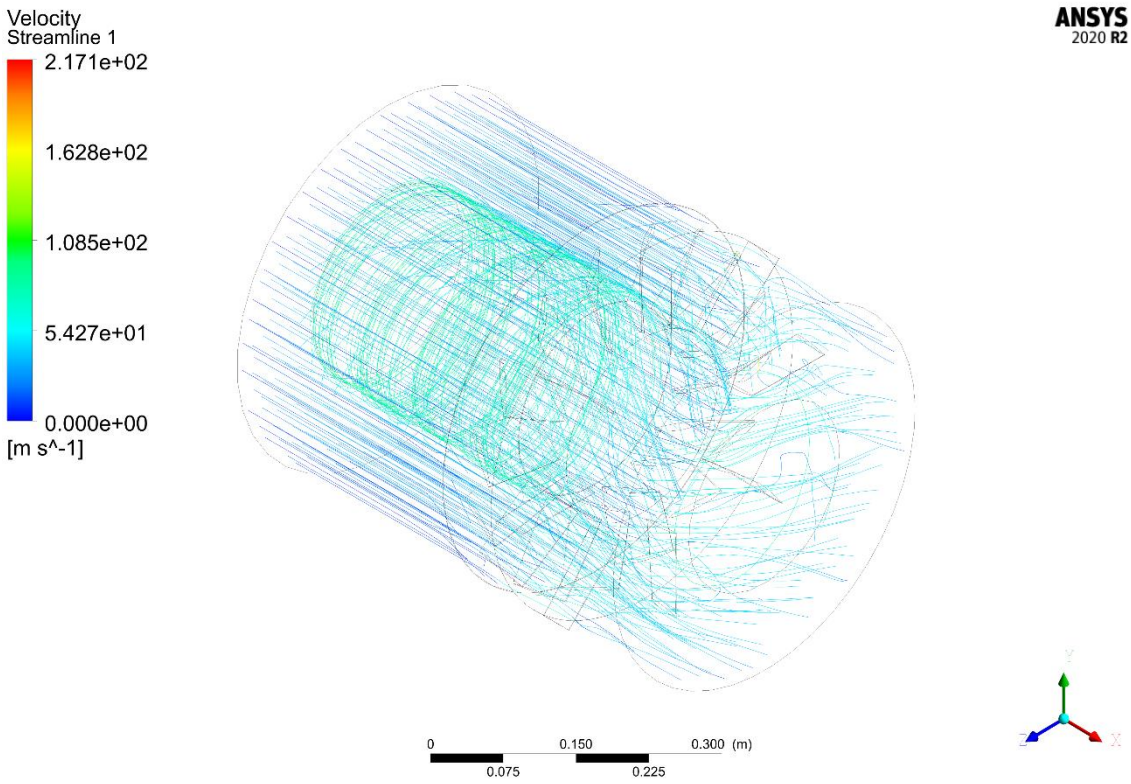

Figure 4.5 Velocity streamline

Referring to Figure 4.3, we can observe the variation of total pressure throughout the flow domain. Total pressure has increased in the region near the rotor. This is due to the acceleration of flow by the rotor which in turn gave rise to the dynamic pressure. The dynamic pressure decreases significantly in the stator, the stator being stationery. However, static pressure at the stator has increased at the expense of flow velocity which can be visualized in Figure 4.4. Absolute velocity of flow past the rotor has been decreased indicating diffusion at the rotor. In the stator, the velocity of flow has been decreased as expected giving rise to the static pressure. The deviation of flow through the rotor and stator can be visualized by the velocity streamline shown in Figure 4.5.

Considering the flow at the inlet and just past the stator, the rise in total pressure is found to be 1.1 which is slightly less than our hand calculation.

CHAPTER FIVE: CONCLUSION

In this way, a single-stage axial-flow compressor was designed following preliminary analysis and CFD simulation. The designed compressor has a pressure ratio of 1.1. The pressure ratio in the case of axial flow compressor is limited due to adverse pressure gradient. Therefore, obtaining a higher pressure ratio would be a challenge as it results in flow separation. In our project, however, an attempt to analyze boundary flow is limited by the meshing size. In future studies, a more refined mesh should be constructed to analyze flow in the axial flow compressor more efficiently.

REFERENCES

Bloch, G. S., & O'Brien, W. F. (1992). A wide-range axial-flow compressor stage performance model. In *Turbo Expo: Power for Land, Sea, and Air* (Vol. 78934, p. V001T01A025).

Boyce, M. P. (2012). Axial-flow compressors. *Gas turbine engineering handbook*, 303-355.

Bringhenti, C., Tomita, J. T., Silva, F. d., & Carneiro, H. F. (2015). One-stage Power turbine preliminary design and analysis. *Journal of Aerospace Technology and Management, 7*, 157--169.

Chen, L., Sun, F., & Wu, C. (2005). Optimum design of a subsonic axial-flow compressor stage. *Applied energy, 80*, 187--195.

Chen, N. (1995). A comparative study on different leaned and skewed bladings in a turbine stator by 3-D Navier-Stokes analysis. *Fluid Dynamics Conference*.

Falck, N. (2008). *Axial compressor mean line design.* Sweden: Lund University.

Gambini, M., & Vellini, M. (2020). *Turbomachinery: Fundamentals, Selection and Preliminary Design.* Springer Nature.

Gu, C.-g., & Miao, Y.-m. (1987). Blade Design of Axial-Flow Compressors by the Method of Optimal Control Theory—Physical Model and Mathematical Expression.

Kim, H.-J., Noh, H.-J., & Kim, Y.-J. (2018). Optimal Design of Rotor Blades for an Axial Compressor Using the Gradient Based Method. *International Conference on Engineering Optimization*, 498-509.

Komarov, O. V., Sedunin, V. A., & Blinov, V. L. (2014). Application of optimisation techniques for new high-turning axial compressor profile topology design. In *Turbo Expo: Power for Land, Sea, and Air* (Vol. 45615, p. V02BT39A008).

Kumar, S. S., Kumar, L., Kumaran, R. S., Kumar, V. S., & Shobhavathy, M. (2019). Design of High Transonic Axial Compressor Stage for Small Gas Turbine Applications. *Gas Turbine India Conference. 83525.* American Society of Mechanical Engineers.

Lee, S.-Y., & Kim, K.-Y. (2000). Design optimization of axial flow compressor blades with three-dimensional Navier-Stokes solver. *KSME International Journal, 14*, 1005--1012.

Lee, S.-Y., & Kim, K.-Y. (2000). Design optimization of axial flow compressor blades with three-dimensional Navier-Stokes solver. *KSME International Journal, 14*, 1005--1012.

Lyons, W. C. (2009). Air and Gas Drilling Manual: Applications for Oil and Gas Recovery Wells and Geothermal Fluids Recovery Wells.

Madadi, A., Kermani, M., & Nili, M. (2015). Three-Dimensional Design of Axial Flow Compressor Blades Using the Ball-Spine Algorithm. *Journal of Applied Fluid Mechanics, 8*.

Mamidoju, C. (2014). Computational Analysis Of A Multistage Axial Compressor.

Massardo, A., & Satta, A. (1990). Axial flow compressor design optimization: Part I—Pitchline analysis and multivariable objective function influence.

Rechter, H., Steinert, W., & Lehmann, K. (1985). Comparison of controlled diffusion airfoils with conventional NACA 65 airfoils developed for stator blade application in a multistage axial compressor.

Sehra, A., Bettner, J., & Cohn, A. (1992). Design of a high-performance axial compressor for utility gas turbine.

Simoes, M. R., Montojos, B. G., Moura, N. R., & Su, J. (2009). Validation of turbulence models for simulation of axial flow compressor. In *20th international congress of mechanical engineering.*

Ujjawal, A. J., & Joshi, S. I. (2013). Design and analysis of stator, rotor and blades of the axial flow compressor. *International Journal of Engineering Development and Research*, 24-29.

Wanjin, H., Zhongqi, W., Chunqing, T., Hong, S., & Mochun, Z. (1994). Effects of leaning and curving of blades with high turning angles on the aerodynamic characteristics of turbine rectangular cascades.

APPENDIX A: MATLAB CODE

main.m

```
clc
close all;
clear all;

%Initial parameters
design_coefficients = [0.8,0.4,0.61];%degree of reaction, work coefficient,
flow coefficient
flowcoef = design_coefficients(3);
m =  4.91;
RPM =10000; %Check this value %for 10000 mach 0.5 at mean
hubtotip = 0.5;
presure =101325;
tem = 288;
rho = 1.225;

%Flow angle at mean
    a1 = 0;
    a2 = 30.13;
    b1 = -58.61;
    b2 = -44.52;
   flowang =[0,30.13,-58.61,-44.52]; %a1, a2, b1, b2

%Axial velocity calculation
Axi_vel = axial_velocity(m,RPM,hubtotip,flowcoef,a1,50); %gives axial
velocity, root mean and tip radius
ca = Axi_vel(1);%axial velocity
r = [Axi_vel(2), Axi_vel(3), Axi_vel(4)];  %root mean tip
rr = Axi_vel(2);%root radius
rm = Axi_vel(3);%mean radius
rt = Axi_vel(4); %tip radius
span = rt-rr;
tipclearance = 0.05*span;
inlet_radius = rt + tipclearance;
fprintf("Span = %.3f\nTip clearance = %.3f\nInlet radius =
%.3f\n\n",span,tipclearance,inlet_radius);
%Velocity triangle
veltr(ca,flowang,RPM,r);
%Blade calculation
mid =[58.61,44.52,1.103928]; %b1,b2,sigma
hub =[47.81,13.11,1.697653];
```

```
tip =[65.42,60.26,0.848826];
fprintf("Blade calculation at mean\n\n")
blade_angle(mid);
fprintf("Blade calculation at hub\n\n")
blade_angle(hub);
fprintf("Blade calculation at tip\n\n")
blade_angle(tip);
fprintf("Stator angles:\n\n")
mid_s = [a2,a1,0.3527];
fprintf("Blade calculation at mean\n\n")
blade_angle(mid_s);
hub_s = [41.04,0,0.5730];
fprintf("Blade calculation at hub\n\n")
blade_angle(hub_s);
tip_s = [23.52,0,0.2865];
fprintf("Blade calculation at tip\n\n")
blade_angle(tip_s);
```

axial_velocity.m- Function which calculates the axial velocity of flow.

```
function axi_vel = axial_velocity(m,RPM,hubtotip,flowcoef,alpha,Ca)
axi_vel = [];
 while true
    C = Ca/cosd(alpha);
%     T = T0 - C^2/(2*cp);
%     P = P0*(T/T0)^(gamma/(gamma -1));
%     rho = P/(R*T)
    rho = 1.225;
    rt = sqrt(m/(pi*rho*Ca*(1-hubtotip)^2)); %tip radius
    rr = rt * hubtotip; %root radius
     rm = (rt+rr)/2;
     Um = 2*pi*rm*RPM/60;
%     rrms = sqrt((rt^2+rr^2)/2);
%     Urms = 2*pi*rrms*RPM/60;
%     Ca_n = Urms*flowcoef   %new axial velocity
     Ca_n = Um*flowcoef; %new axial velocity
    if abs(Ca - Ca_n) <= 0.01
        break;
    end
    Ca = Ca_n;
 end
```

```
 axi_vel = [Ca_n,rr,rm,rt];
 fprintf("\nAxial velocity = %.3f\nrm = %.3f\nr_hub = %.3f\nr_tip =
%.3f\n\n",Ca_n,rm,rr,rt);
end
```

veltr.m – Function which calculates component of velocity triangle and other geometric parameters of both rotor and stator.

```
function vel_tri= veltr(ca,flowang,N,r)
   vel_tri = [];
   omega = 2*pi*N/60;
   a = sqrt(1.4*287*288); %speed of sound
   r_hub =r(1);
   rm = r(2);
   r_tip = r(3);

   %Velocity Triangle at mean
    a1 = flowang(1);
    a2 = flowang(2);
    b1 = flowang(3);
    b2 = flowang(4);

    %Three velocity component at inlet and exit
    c1 = ca/cosd(a1);
    c2 = ca/cosd(a2)
    w1 = ca/cosd(b1)
    w2 = ca/cosd(b2)
    ct1 = ca*tand(a1);
    wt1 = ca*tand(b1)
    ct2 = ca*tand(a2);
    wt2 = ca*tand(b2)
    u = omega * rm;
    fprintf("\n\nVelocity triangle component at mean\nu = %.3f\nAt inlet\nC1
= %.3f\nW1 = %.3f\nCt1 = %.3f\nWt1 = %.3f\n",u,c1,w1,ct1,wt1);
    fprintf("At outlet\nC2 = %.3f\nw2 = %.3f\nct2 = %.3f\nwt2 =
%.3f\n",c2,w2,ct2,wt2);
    %Normalized component of velocity triangle
    U = u/u;
    C1 = c1/u;
    C2 = c2/u;
    W1 = w1/u;
```

```
    W2 = w2/u;

    Work = u*(ct2-ct1);
    %Mach numbers
    Ma = ca/a
    Mt = u/a
    Mr = sqrt(Ma^2+Mt^2)
    %For checking degree of reaction
    R = 0.5-((ca/(2*u))*(tand(a1) + tand(b2)));

    if abs(R - 0.8 ) <1
        fprintf("\nComponent of velocity triangles for a given parameter
gives similar value of R as initialized.\nInitial value of R =
0.8\nCalculated value of R = %0.3f\n\n", R);
    end

    %For checking flow coefficient
    phi = ca/u;

    if abs(phi - 0.61 ) <1
        fprintf("\nComponent of velocity triangles for a given parameter
gives similar value of Phi as initialized.\nInitial value of Phi =
0.61\nCalculated value of Phi = %0.3f\n\n", phi);
    end
    %For checking work coefficient
%     psi = 1+((ca/u)*(tand(b2)-tand(a1)));
    psi = (ct2-ct1)/u;
    if abs(psi - 0.4) <1
        fprintf("\nComponent of velocity triangles for a given parameter
gives similar value of Psi as initialized.\nInitial value of psi =
0.4\nCalculated value of Phi = %0.3f\n\n", psi);
    end


    %Checking for method to calculate solidity
    ratio = w2/w1;
    if ratio >= 0.658
        fprintf("\nThe ratio of relative velocity W2/W1 is greater than
0.658\nTherefore use Mckenize method to calculate solidity.\n\n");
    else
        fprintf("\nError!!!\nThe ratio of relative velocity W2/W1 is  not
greater than 0.658\nCannot use Mckenize method to calculate solidity.\n\n");
    end
```

```
    %Calculating relative Mach number

    if Mr < 0.7
        fprintf("\nMr(mean) = %.3f\nRelative mach number is less than 0.7 at
mean\nCan use NACA 65 series airfoil\n\n",Mr);
    else
        fprintf("\nError in relative Mach Number!!!!!!!!!!!!!!\nMach number
greater than 0.7 at mean. Flow might be transonic at tip.\n\n");
    end

    %chord
     AR = 1.5; %Aspect ratio
%     Q = m/rho %Mass flow rate
%     A = Q/c1 %Annulus area
%     hb = A/(2*pi*rm) %Blade height
%     c = hb/AR

    %chord
    chord  = (r_tip-r_hub)/AR;


    %solidity
    Cp = 1-(w2/w1)^2;
    inv_sigma = 9*(0.567-Cp); %1/solidity
    S = chord*inv_sigma; %spacing
    num = (2*pi*rm)/S;%number of blades
    nr = ceil(num);
    fprintf("Solidity = %f\nSpacing between the blades = %f\nNumber of blades
= %d\n\n",1/inv_sigma,S,nr);

    %Free vortex law
    ct2_tip = (ct2*rm)/r_tip;
    ct2_hub = (ct2*rm)/r_hub;

    %Velocity triangle at hub
    u_hub = r_hub*omega;
    %At inlet
    c1_hub = c1
    a1_hub = 0;
    b1_hub = -atand(u_hub/ca); %tan(alpha) = 0
    w1_hub = ca/cosd(b1_hub)
    wt1_hub = ca*tand(b1);
```

```
    %At outlet
    a2_hub = atand(ct2_hub/ca);
    b2_hub = atand((u_hub/ca)-tand(a2_hub));
    w2_hub = ca/cosd(b2_hub)
    c2_hub = ca/cosd(a2_hub)

    %solidity and spacing
    S_hub = 2*pi*r_hub/nr;
    sigma_hub = (nr*chord)/(2*pi*r_hub);
    Mt_hub = u_hub/a
    Mr_hub = sqrt(Ma^2+Mt_hub^2);
    fprintf("\nParameter at hub\na1 = %.2f\na2 = %.2f\nb1 = %.2f\nb2 =
%.2f\nU = %.2f\nSolidity =
%f\n",a1_hub,a2_hub,b1_hub,b2_hub,u_hub,sigma_hub);
    %velocity triangle at mid
    fprintf("\nParameter at mid\na1 = %.2f\na2 = %.2f\nb1 = %.2f\nb2 =
%.2f\nU= %.2f\n",a1,a2,b1,b2,u);
    fprintf("\nRelative Mach number at hub = %.3f\n",Mr_hub);


    %Velocity triangle at tip
    u_tip = r_tip*omega;
    %At inlet
    c1_tip = c1
    a1_tip = 0;
    b1_tip = atand(u_tip/ca); %tan(alpha) = 0
    w1_tip = ca/cosd(b1_tip)
    %At outlet
    a2_tip = atand(ct2_tip/ca);
    b2_tip = atand((u_tip/ca)-tand(a2_tip));
    w2_tip = ca/cosd(b2_tip)
    c2_tip = ca/cosd(a2_tip)

    %solidity and spacing
    S_tip = 2*pi*r_tip/nr;
    sigma_tip = (nr*chord)/(2*pi*r_tip);
    %Relative Mach number
    Mt_tip = u_tip/a
    Mr_tip = sqrt(Ma^2+Mt_tip^2);
    fprintf("\nParameter at tip\na1 = %.2f\na2 = %.2f\nb1 = %.2f\nb2 =
%.2f\nU= %.2f\nSolidity = %f\nSpacing =
%.3f\n",a1_tip,a2_tip,b1_tip,b2_tip,u_tip,sigma_tip,S_tip);
    fprintf("\nRelative Mach number at tip = %.3f\n",Mr_tip);
```

```
c3 = ca;
%for stator
ARS = 2.5;
cs = (r_tip-r_hub)/ARS
cpd = 1 - (c3/c2)^2;
SigmaS  = 1/(9*(0.567-cpd))
s = cs/SigmaS;
Ns = (2*pi*rm)/(s)
ns = ceil(Ns);
axial_distance = 0.2-chord

%tip
Ss_tip = 2*pi*r_tip/ns;
sigmas_tip = (ns*cs)/(2*pi*r_tip)
%hub
Ss_hub = 2*pi*r_hub/ns;
sigmas_hub = (ns*cs)/(2*pi*r_hub)
```

APPENDIX B: CHARTS

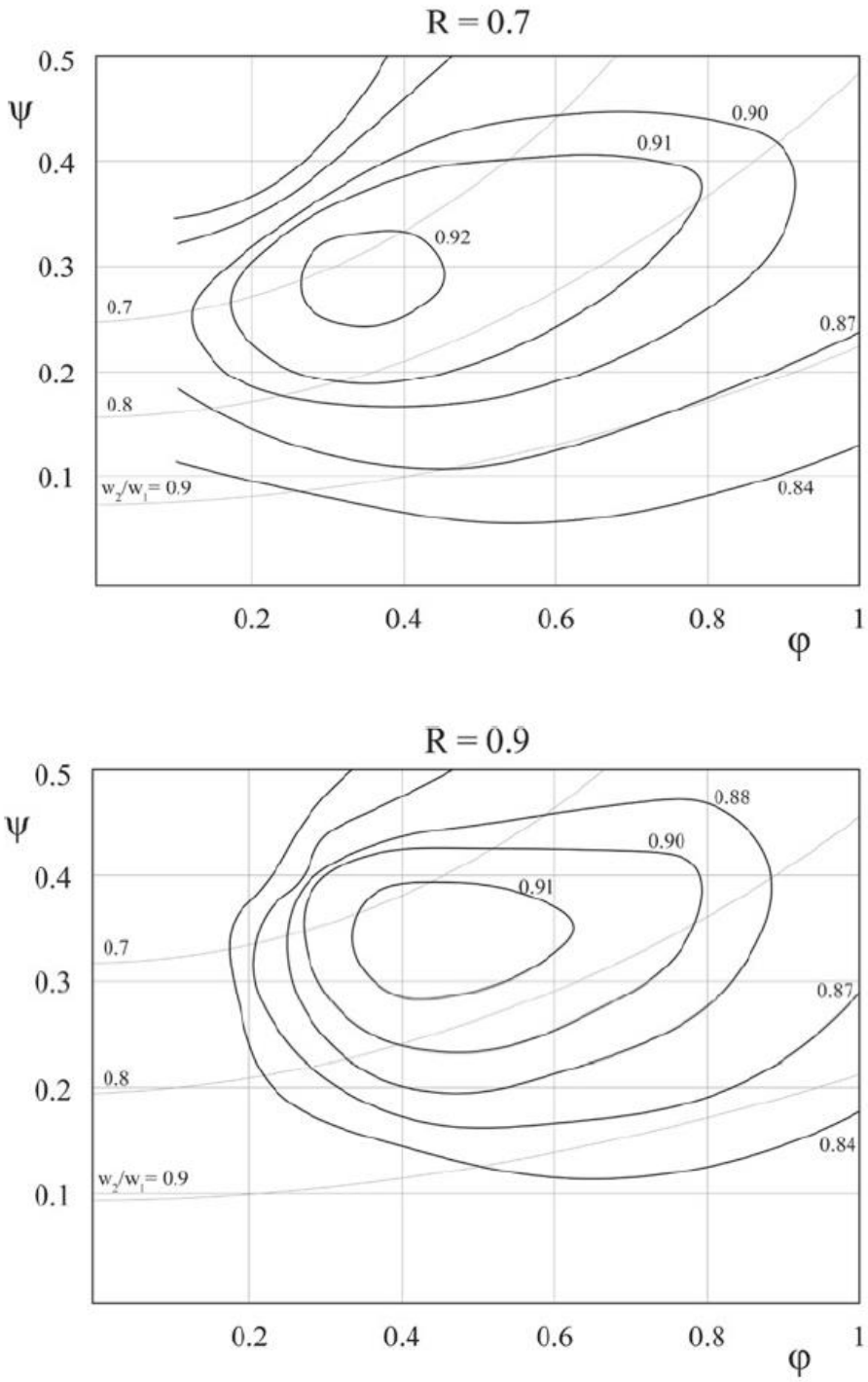

Figure B.1 Smith Diagram for axial flow compressor

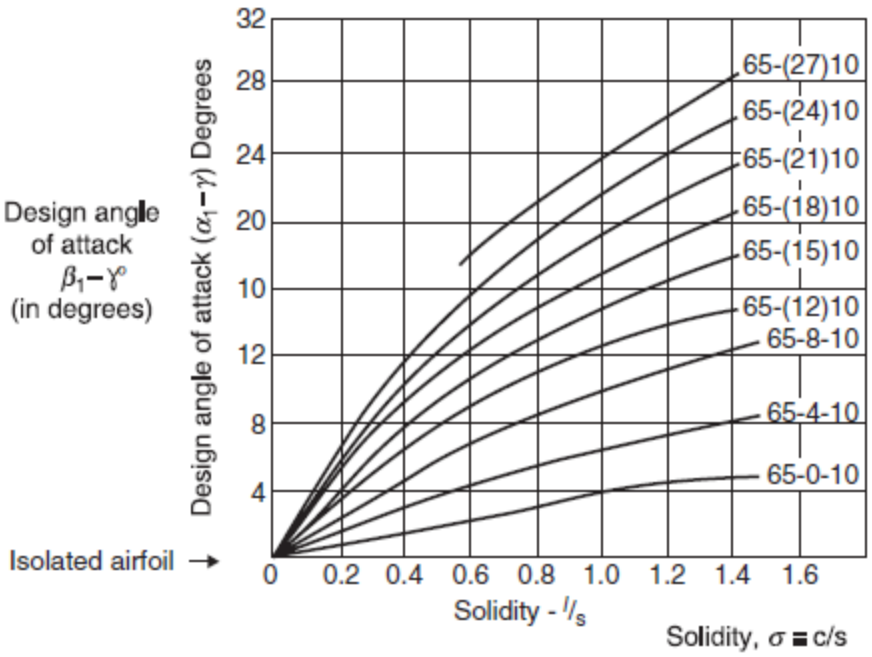

Figure B.2 Design angle of attack for 65-series airfoil with 10% thickness as a function of solidity.

Source: Herrig, Emery, and Erwin 1951

APPENDIX C: AIRFOIL DATA

Rotor and Stator Blade Airfoil

Table C.1 Airfoil data of NACA 65-410

X(mm)	Y(mm)	X(mm)	Y(mm)
100	0	0.628	-0.661
95.029	0.937	0.893	-0.781
90.057	1.842	1.411	-0.944
85.076	2.729	2.682	-1.191
80.088	3.577	5.203	-1.536
75.09	4.372	7.711	-1.791
70.085	5.099	10.212	-1.999
65.073	5.741	15.202	-2.314
60.053	6.288	20.183	-2.547
55.029	6.72	25.157	-2.71
50	7.018	30.128	-2.814
44.968	7.153	35.097	-2.863
39.936	7.138	40.064	-2.854
34.903	6.983	45.032	-2.773
29.872	6.702	50	-2.606
24.843	6.29	54.971	-2.34
19.817	5.731	59.947	-2.004
14.798	5.006	64.927	-1.621
9.788	4.067	69.915	-1.211
7.289	3.487	74.91	-0.792
4.797	2.8	79.912	-0.393
2.318	1.935	84.924	-0.037
1.089	1.372	89.943	0.226
0.607	1.061	94.971	0.327
0.372	0.861	100	0
0	0		